MR and MR angiography of Sturge-Weber syndrome.

T J Vogl, J Stemmler, C Bergman, T Pfluger, E Egger and J Lissner

AJNR Am J Neuroradiol 1993, 14 (2) 417-425
http://www.ajnr.org/content/14/2/417

MR and MR Angiography of Sturge-Weber Syndrome

Th. J. Vogl,[1] J. Stemmler,[1] C. Bergman,[1] Th. Pfluger,[1] E. Egger,[2] and J. Lissner[1]

PURPOSE: To assess the potential of magnetic resonance angiography (MRA) as an adjunct to spin-echo sequences in evaluating the cerebral vascular anomalies seen in Sturge-Weber syndrome. **METHODS**: Four pediatric patients with Sturge-Weber syndrome were evaluated with conventional MR imaging and with arterial and venous MRA. Resultant images were evaluated for evidence of volume loss, cortical enhancement, vascular anomalies, and enlarged choroid plexus. **RESULTS**: Venous MRA revealed reduced flow of the transverse sinuses and jugular veins, prominent deep collateral venous system, and a lack of superficial cortical veins. Arterial MRA, performed in all cases, revealed a reduced flow signal from the left middle cerebral artery in one hemiparetic patient and angiomatous changes of high branches of a middle cerebral artery in two patients. **CONCLUSION**: Arterial and, in particular, venous MRA can be useful adjuncts to standard spin-echo sequences in diagnosing Sturge-Weber syndrome.

Index terms: Phakomatoses; Magnetic resonance angiography (MRA); Magnetic resonance, in infants and children

AJNR 14:417-425, Mar/Apr 1993

The Sturge-Weber syndrome is a phakomatosis characterized by trigeminal port-wine facial nevus (encephalotrigeminal angiomatosis), pial venular angioma (usually ipsilateral to the facial nevus), intracranial calcifications, seizures, cerebral atrophy, mental retardation, hemiparesis, glaucoma, and buphthalmos (1).

Magnetic resonance (MR) allows good delineation of abnormalities in gray and white matter, and—with the use of contrast media such as Gd-DTPA—visualization of abnormalities of the pia has become possible. MR imaging effectively demonstrates leptomeningeal enhancement after contrast medium administration, parenchymal loss, and choroid plexus enlargement on pre- and postcontrast scans. MR is better able to demonstrate vascular anomalies, while computed tomography (CT) is more sensitive in evaluating calcifications.

Received November 26, 1991; revision requested January 28, 1992; final revision received June 6 and accepted June 12.

Presented at the 77th Scientific Assembly and Annual Meeting of the RSNA, December 1–6, 1991, Chicago, IL.

[1] Department of Radiology, University of Munich, Ziemssenstrasse 1, 8000 Munich 2, Germany. Address reprint requests to PD Dr med habil Th. J. Vogl.

[2] Hauner'sches Kinderspital, University of Munich, Germany.

AJNR 14:417-425, Mar/Apr 1993 0195-6108/93/1402-0417

The development of MR angiography (MRA) has allowed direct visualization of flow signal from the engorged deep medullary venous system and changes in the intracranial arterial system in the Sturge-Weber syndrome, changes that before could be seen only as signal voids on spin-echo (SE) sequences. The direct visualization of the pathognomonic pial angioma, however, remains elusive in CT, MR, and conventional angiography. We report our experience with MR and MRA in detecting typical intracranial vascular anomalies in four patients with Sturge-Weber syndrome.

Materials and Methods

Four female pediatric patients with Sturge-Weber syndrome, aged 1, 2, 3, and 10 years, were evaluated with MR and MRA, performed with a Magnetom 1.5-T superconducting magnet, using a circular polarized head coil.

We used the following SE sequences: T2-weighted (TR/TE = 2500/22, 60, 90) in axial orientation, and T1-weighted (500/15) in sagittal and/or axial before and after application of the contrast medium Gd-DTPA (0.1 mmol/kg intravenously).

Arterial MRA was performed using 3-D Fourier transformed, rephased gradient-echo recalled FISP (fast imaging with steady precession) 3-D sequences, with the following parameters: TR/TE = 40/7, α = 15°, thickness 40–96 mm, field of view 200 mm, one acquisition, 64 3-D overlapping partitions, effective section thickness = 1.5 mm,

TABLE 1: Summary of clinical, ultrasound, and CT findings in four patients with Sturge-Weber syndrome

	Case 1 S.J., f, 3 years old	Case 2 K.C., f, 1 year old	Case 3 Z.K., f, 10 years old	Case 4 B.H., f, 2 years old
Facial nevus	Left-sided facial nevus cranial nerve V (1, 2)	Bilateral facial nevus	Left-sided facial nevus	Left-sided mutiple nevi
Neurologic findings	Right-sided: seizures; hemiparesis Left-sided: hemianopia mental retardation	Right-sided: seizures; hemiparesis Bilateral: extrapyramidal signs Mental retardation	Right-sided: seizures; hemiparesis; paresis cranial nerve: VII, XII Apraxia	Left-sided: seizures
Other findings	Microcephalus	Microcephalus		Right-sided: megalencephaly
Cranial CT	Not performed	Right-sided: calcification frontal lobe Bilateral: cerebral atrophy	Left-sided: calcification frontotemporal; cortical atrophy	Left-sided: calcification paramedian; cortical enhancement; dilated ventricle system

TABLE 2: Summary of MR and MRA findings in four patients with Sturge-Weber syndrome

	Case 1 S. J., f, 3 years old	Case 2 K. C., f, 1 year old	Case 3 Z. K., f, 10 years old	Case 4 B. C., f, 2 years old
SE sequences				
Volume loss	Left-sided hemiatrophy	Left > right-sided hemiatrophy	Left-sided hemiatrophy	Left-sided hemiatrophy
Choroid plexus	Enlarged	Enlarged	Enlarged	Enlarged
Deep venous system	Engorged deep veins	Engorged deep veins	Engorged deep veins	Engorged deep veins
Postcontrast scans (Gd-DTPA)	Left-sided frontotemporal leptomeningeal enhancement	Right-sided frontotemporal and left parietooccipital enhancement	Leptomeningeal enhancement of left hemisphere	Left-sided frontotemporal leptomeningeal enhancement
Arterial MRA	Right-sided pial blush	Angiomatous changes (MRA after Gd-DTPA)	Signal loss left middle cerebral artery	Angiomatous changes of right middle cerebral artery
Venous MRA	Signal loss left transverse sinus, prominent vein of Labbe and ascending veins	Not performed	Signal loss left jugular vein Collateral veins	Prominent deep venous system Lack of superficial veins Septated transverse sinus on the left

matrix 256 × 256, transverse orientation, two saturation pulses.

Venous MRA images were obtained with FLASH (fast low angle shot) 2-D sequences using the following parameters. TR/TE = 36/10, $\alpha = 60°$, 53 sections, thickness 3–10 mm, section gap = −0.3 mm, field of view 200 mm, one acquisition, matrix 256 × 256, coronal orientation, one saturation pulse. The choice of orientation of the acquisition plane in venous and arterial MRA was based on an empiric study of healthy volunteers in which axial acquisition for arterial, and coronal acquisition for venous MRA produced the best results.

The 2-D or 3-D data sets were processed using a computer ray tracing algorithm on an integrated work station to achieve maximum intensity projection images.

We evaluated the clinical findings, cranial CT findings, the conventional SE MR images, and maximum intensity projection-processed MRA images as well as the individual sections from which the maximum intensity projection images were constructed.

Results

Our clinical findings (see Tables 1 and 2) corresponded well with the extensively documented characteristics of Sturge-Weber syndrome. All four of our patients presented with unilateral or, in one case, bilateral facial nevi and neurologic findings in the form of generalized epileptic seizures and, in three cases, hemiparesis. In addition, one patient presented with bilateral, extrapyramidal signs; in another case, facial and hypoglossal paralysis and apraxia were evident. Ophthal-

mologic examinations revealed left-sided hemianopia in one case. An assessment of mental capacity demonstrated mental retardation in two cases; these patients had microcephaly as well. In a third patient, a formal IQ test gave borderline results. In one case, there was a right-sided megalencephalic skull with contralateral dilated ventricle system and multiple left-sided facial nevi. In all four patients, delayed physical development was evident.

Cranial CT examination had been performed in three patients as part of the initial work-up, revealing pathognomonic intracranial calcifications and signs of cerebral atrophy in all. In one case performed with contrast medium, spotty enhancement of large portions of the cortex was seen additionally (see Fig. 4A).

In our four patients, MR imaging presented a spectrum of characteristic findings. On SE sequences, volume loss in the form of hemiatrophy was seen in three patients (Fig. 1A), and bilateral atrophy in one. Both abnormal cortical substance and abnormal white matter appeared isointense with respect to corresponding areas of the normal hemisphere on precontrast T1-weighted images (Figs. 1A, 2A, and 3A). On postcontrast T1-weighted images, the abnormal cortex and white matter appeared hyperintense (Fig. 1B), except for one case in which the white matter of the involved hemisphere appeared isointense in comparison with normal tissue.

In all four patients, a bilaterally enlarged glomus of the choroid plexus was seen, producing increased signal intensity on postcontrast T1-weighted images (Figs. 2B and 2C).

In each case, conventional MR revealed engorged deep vessels on pre- and postcontrast T1-weighted images in the form of signal voids (Figs. 1A, 1B, 2A, 2B, 3A, 3B, and 4C).

T2-weighted images showed hyperintensity of the affected cortical areas, corresponding to the enhanced areas after contrast material application on T1-weighted images. In one patient, calcification of the choroid plexus was visible as an area of decreased signal intensity on the T2-weighed scan, corresponding to the cranial CT finding (Fig. 4B).

To evaluate vascular anomalies, we performed venous and arterial MRA. Arterial MRA, performed on each patient, showed in one case a loss of flow signal from the left middle cerebral artery, which corresponded clinically to the patient's right-sided hemiparesis (Figs. 3F and 3G). In two other cases, high cortical branches of the middle cerebral artery, ipsilateral to the affected cortex, showed subtle but conspicuous changes. In one of these cases, frank angiomatous changes were evident (Fig. 1D); in the other, a pial blush could be appreciated (Fig. 1C). In one case, arterial MRA was performed after contrast injection; angiomatous changes with influx from both posterior cerebral arteries could be seen (Figs. 2C and 2D).

Venous MRA, performed on three patients, revealed pathologic changes in the form of engorged deep medullary veins in each case. There was a lack of flow signal from the left transverse sinus in two cases (Figs. 1E and 1G). In one of these a venous flow from deep medullary veins through collaterals to an engorged vein of Labbé, with nearly absent ascending cortical veins, was visible (Figs. 1C and 1G). In the other case, engorged deep collateral veins could be seen. (Figs. 3D and 3G). In one case, a lack of superficial veins, and a septum at the transition from the left transverse into the sigmoid sinus, was seen (Figs. 4D and 4E). In each case in which venous MRA revealed engorged deep hemispheric veins, there was a marked reduction in prominence of the superficial veins of the same hemisphere.

Discussion

Sturge-Weber syndrome is a phakomatosis that was initially described by Sturge in 1879. Weber demonstrated the characteristic and pathognomonic intracranial calcifications on skull films in 1922 (3, 4). Since that time many details and variants of the syndrome have been elucidated.

The diagnosis of Sturge-Weber syndrome can be made using CT in most cases, albeit indirectly, and is based on signs such as intracranial calcifications, enlarged choroid plexus and cortical enhancement on postcontrast scans, and an abnormal deep venous system. CT has an advantage in comparison with MR in the evaluation of calcified areas when using conventional SE sequences, but MR has been reported to reveal intracranial calcification as effectively as CT when using appropriate gradient-echo sequences [5, 6).

Choroid plexus enlargement is typical in Sturge-Weber syndrome (7). On plain MR images, the signals from the choroid plexus do not show consistent intensity but may appear hypo-, iso-, or hyperintense. In each of our four cases, the size of the choroid plexus glomus was greater than 10 mm bilaterally (normal at age 6–10: 2.5

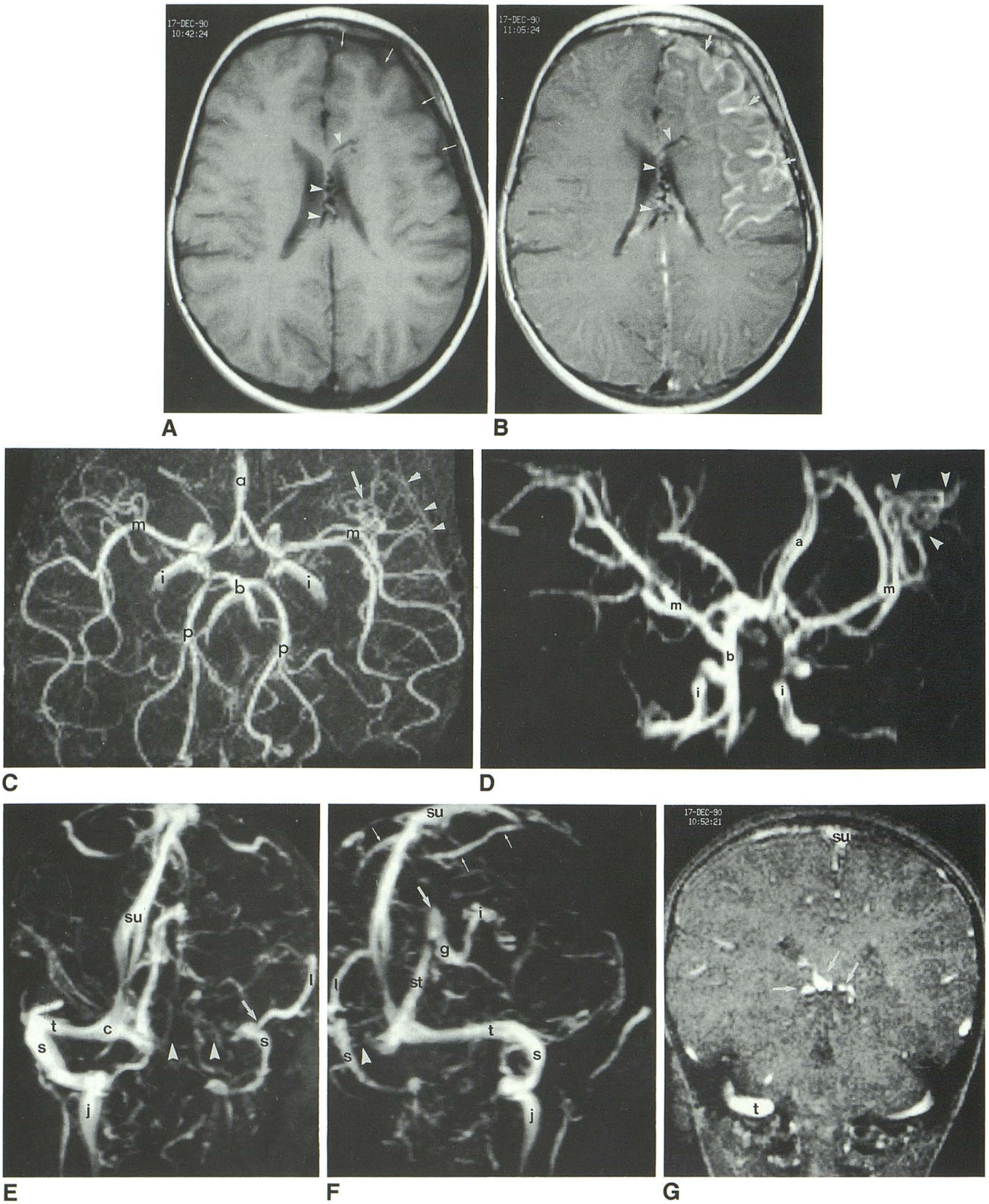

Fig. 1. Case 1. This 3-year-old mentally retarded patient presented with left-sided facial nevus and hemianopia, and right-sided seizures and hemiparesis. (*Continued on next page.*)

mm) (8), and showed a hyperintense signal on postcontrast T1-weighted images.

Cortical and leptomeningeal enhancement of the affected cortex after injection of contrast medium is seen on CT as well as MR images. This enhancement is thought, on the one hand, to be due to blood-brain barrier disruption resulting from the ischemia of repeated, therapy-refractory seizures (2); other authors have suggested that the area of enhancement represents the pial angioma itself. The latter case is supported by a study that found a correlation between surgical findings and MR images of the corresponding areas (7). Assessing the extent of cortical pathology is prognostically important, since extensive or bilateral angiomatous malformations are often associated with mental retardation and seizures refractory to therapy (9–11). Our study verified these associations, as all four patients showed large areas of cortical enhancement while scoring borderline to low on formal IQ tests.

Vascular anomalies visible on MR images in Sturge-Weber syndrome that have been reported to date include deep hemispheric veins and/or dilated sinus systems, generally seen on conventional SE images as hypointense structures or areas of signal-void. These pathologic vascular findings are in agreement with the findings using conventional angiographic techniques (12–14). The appearance of Sturge-Weber disease using conventional angiography is described in terms of a decreased number of superficial cortical veins in the involved area in addition to enlarged deep medullary veins, which serve as collaterals from the cerebral cortex to the deep veins (14). We consistently found in our patients dilated deep medullary veins in conjunction with a relative paucity of cortical veins in the affected hemisphere. A diffuse persistent staining has been described in conventional angiography as a sign of slow cerebral venous drainage (14). Analogous to this finding, in one of our patients a pial blush on the side of the involved area in arterial MRA could be seen in the MRA sequences. As a nonspecific sign associated with cerebral atrophy, a decreased caliber of the middle cerebral artery branches has been described with conventional angiography. In our study, two other patients showed angiomatous changes of the middle cerebral artery. In one of these cases, we found a loss of flow signal from the left middle cerebral artery in the presence of right-sided hemiparesis. Bizarre venous pathways, such as engorged anastomoses of cortical veins connecting deep medullary veins, have occasionally been found in Sturge-Weber disease (14). In two patients, venous MRA revealed a collateral pathway above an engorged vein of Labbé on the side of the affected cortex. Carotid angiography has often failed to show the superior sagittal sinus, owing to the lack of ascending cortical veins, and the inability of contrast material to reach this sinus. However, in each case of our study in which venous MRA was performed, a rather dilated superior sagittal sinus with high signal intensity was seen. This fact may be an advantage of MRA, because flow signal is independent of ana-

Fig. 1.—*Continued.*

A, SE: T1-weighted, 600/15 (TR/TE), plain, axial image; left-sided hemiatrophy (*arrows*) and engorged deep veins (*arrowheads*) are seen.

B, SE: T1-weighted, 600/15, Gd-DTPA, axial image; the postcontrast scan reveals left frontotemporal leptomeningeal enhancement (*arrows*); the engorged deep venous system is visible as signal voids (*arrowheads*).

C, Arterial MRA, FISP 3D, 40/7, $\alpha = 15°$, axial image; this arterial angiogram suggests a left-sided pial blush (*arrowheads*) and a convolution of vessels of the left middle cerebral artery (*arrow*) (*i*, internal cerebral artery; *a*, anterior cerebral artery; *m*, middle cerebral artery; *b*, basilar artery; *p*, posterior cerebral artery).

D, Arterial MRA, FISP 3D, 40/7, $\alpha = 15°$, axial image; the cor > sag-30° rotated view of the 3-D reconstruction reveals angiomatous changes of cortical branches of the left middle cerebral artery. On postcontrast T1-weighted images, left-sided leptomeningeal enhancement was seen corresponding to this area (*i*, internal cerebral artery; *a*, anterior cerebral artery; *m*, middle cerebral artery; *b*, basilar artery).

E, Venous MRA, FLASH 2D, 36/10, $\alpha = 60°$, coronal image; the cor > sag-15° rotated view of the venous angiogram shows signal loss from the left transverse sinus (*arrowheads*) and an engorged vein of Labbé suggesting collateral venous flow from medullary veins to the sigmoid sinus and jugular vein (*arrow*) (*su*, superior sagittal sinus; *c*, confluens sinuum; *t*, transverse sinus; *s*, sigmoid sinus; *j*, jugular vein; *l*, vein of Labbé).

F, Venous MRA, FLASH 2D, 36/10, $\alpha = 60°$, coronal image; the rotation cor > sag-30° demonstrates prominent deep veins, engorged ascending veins (*short arrows*), and a prominent top of vein of Galen (*arrow*). The collateral venous passage from the engorged vein of Labbé to the jugular vein is visible on the left; there is signal loss from the left transverse sinus (*arrowhead*) (*su*), superior sagittal sinus; *st*, straight sinus; *g*, vein of Galen; *i*, internal cerebral vein; *t*, transverse sinus; *s*, sigmoid sinus; *j*, jugular vein; *l*, vein of Labbé).

G, Venous MRA, FLASH 2D, 36/10, $\alpha = 60°$, coronal image; an individual section from this venous MRA sequence clearly reveals the engorged medullary veins (*arrows*) (*su*, superior sagittal sinus; *t*, transverse sinus).

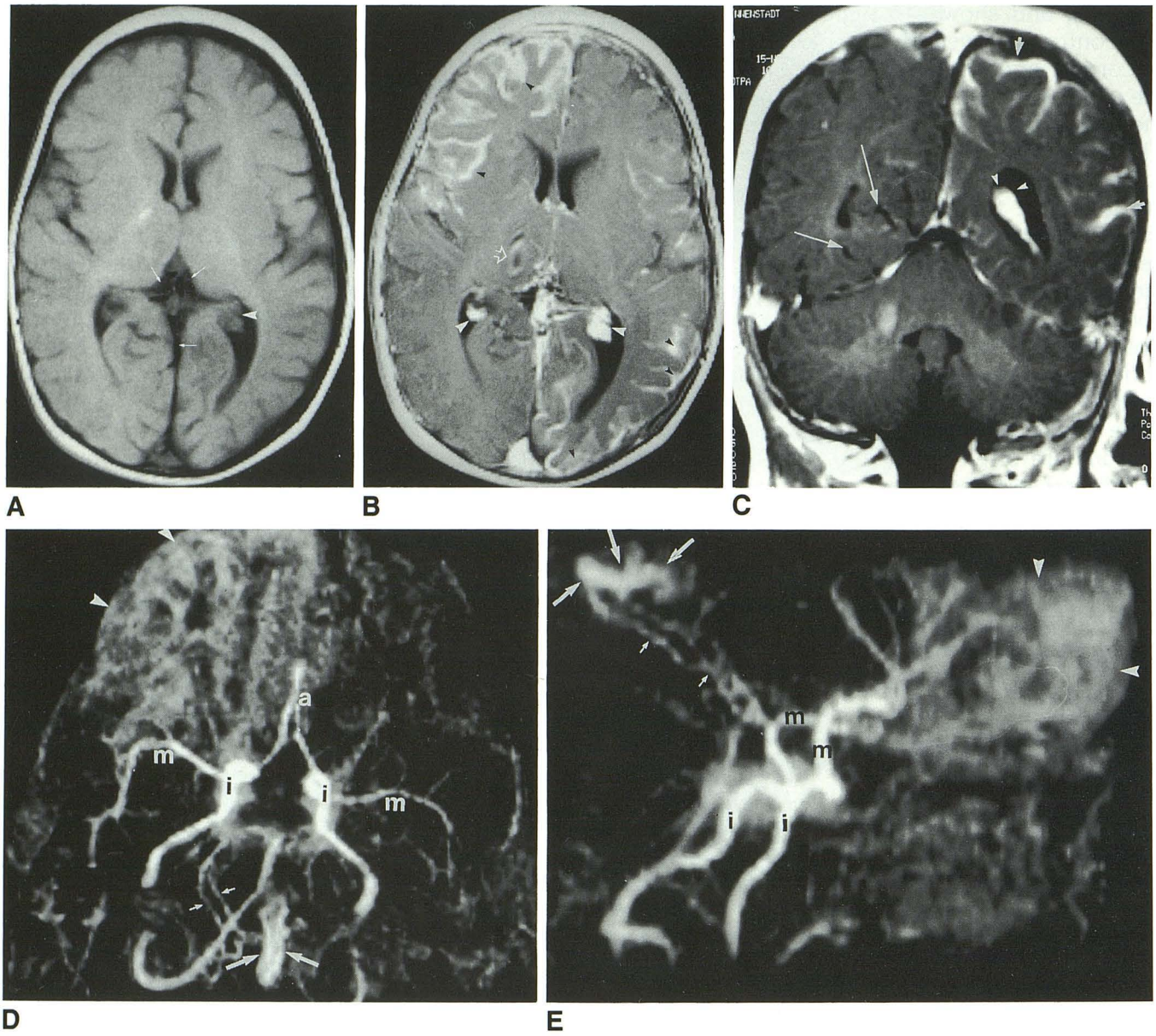

Fig. 2. Case 2. Right-sided seizures and hemiparesis, and a bilateral facial nevus and extrapyramidal signs were clinical findings in this 1-year-old mentally retarded patient.

A, SE, T1-weighted, 600/15 (TR/TE), plain axial image; there are engorged deep veins (*arrows*), and an enlarged glomus of the choroid plexus (*arrowhead*).

B, SE, T1-weighted, 600/15, Gd-DTPA, axial image; there is right frontotemporal and left parietooccipital leptomeningeal enhancement (*black arrowheads*); additionally, high signal from the enlarged glomus of the choroid plexus is shown (*white arrowheads*). Note the flow-related artifact (*open arrow*) arising from a vessel anomaly in this patient.

C, SE, T1-weighted, 600/15 Gd-DTPA, coronal image; leptomeningeal enhancement (*short arrows*), an enlarged glomus of the choroid plexus (*arrowheads*), and engorged deep veins (*long arrows*) are visible.

D, Arterial MRA, FISP 3D, 40/7 $\alpha = 15°$, Gd-DTPA, axial image; the postcontrast angiogram shows right frontal leptomeningeal enhancement (*arrowheads*) and a region of abnormal flow signal in the region of the posterior cerebral artery (*arrows*). Note the influx from the posterior cerebral artery (*short arrows*) (*i*, internal cerebral artery; *a*, anterior cerebral artery; *m*, middle cerebral artery).

E, Arterial MRA, FISP 3D, 40/7, $\alpha = 15°$, Gd-DTPA, axial image; the cor > sag-40° rotated view more clearly reveals the vascular anomaly seen in *D*. Note the angiomatous change (*long arrows*) with influx from the posterior cerebral artery (*short arrows*), and the enhancement of the involved cortical areas (*arrowheads*) (*i*, internal cerebral artery; *m*, middle cerebral artery).

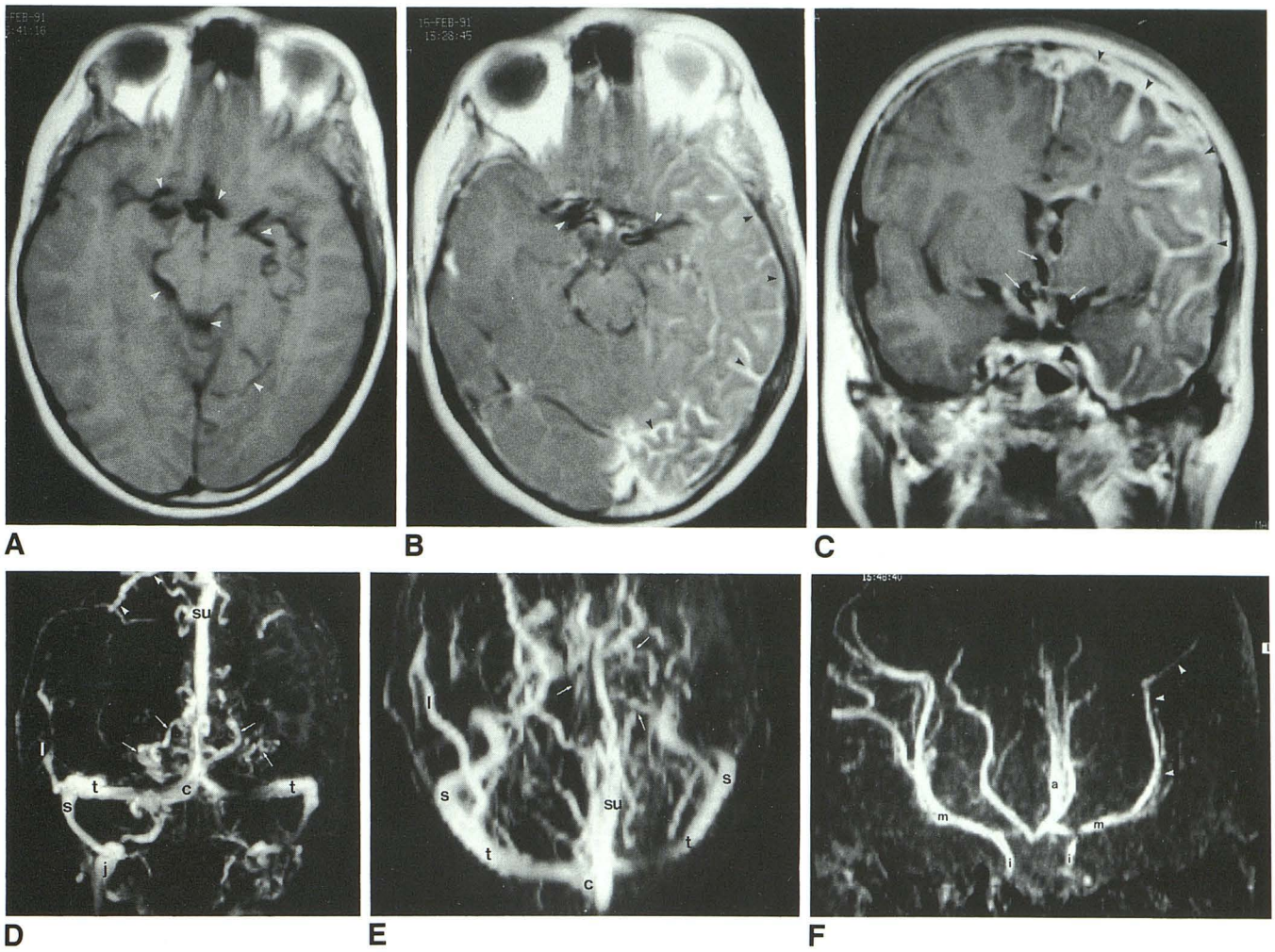

Fig. 3. Case 3. A left-sided facial nevus, and right-sided seizures, hemiparesis and paralysis of cranial nerves VII and XII, and apraxia were findings in this 10-year-old patient.

A, SE, T1-weighted, 600/15 (TR/TE), plain, axial image; the engorged deep venous system in this patient (*arrowheads*) is seen.

B, SE, T1-weighted, 600/15, Gd-DTPA, axial image; the postcontrast scan demonstrates leptomeningeal enhancement of the left hemisphere (*black arrowheads*), and the engorged deep veins (*white arrowheads*).

C, SE, T1-weighted, 600/15, Gd-DTPA, coronal image; an engorged deep venous system (*arrows*) and leptomeningeal enhancement of the left hemisphere (*arrowheads*) can be seen.

D, Venous MRA, FLASH 2D, 36/10, $\alpha = 60°$, coronal image; in addition to the findings on T1-weighted images, the coronal view of the angiogram shows flow signal in a convolution of engorged deep venous vessels (*arrows*). Note the engorged ascending veins on the side contralateral to the affected cortex (*arrowheads*) (*su*, superior sagittal sinus; *c*, confluens sinuum; *t*, transverse sinus; *s*, sigmoid sinus; *j*, jugular vein; *l*, vein of Labbé).

E, Venous MRA, FLASH 2D, 36/10, $\alpha = 60°$, coronal image; the tranverse view of a coronally acquired MRA shows the engorged deep medullary veins (*arrows*) and an engorged vein of Labbé (*su*, superior sagittal sinus; *c*, confluens sinuum; *t*, transverse sinus; *s*, sigmoid sinus; *l*, vein of Labbé).

F, Arterial MRA, FISP 3D, 40/7, $\alpha = 15°$, axial image; this axially acquired MRA, seen in predominantly coronal projection, reveals greatly reduced flow signal from the entire left middle cerebral artery (*arrowheads*), corresponding to the clinical finding of right-sided hemiparesis (*i*, internal cerebral artery; *a*, anterior cerebral artery; *m*, middle cerebral artery).

G, Arterial MRA, FISP 3D, 40/7, $\alpha = 15°$, axial image; the axial view also demonstrates absence of cortical branches of the left cerebral artery (*arrowheads*) in comparison with the right (*a*, anterior cerebral artery; *m*, middle cerebral artery; *p*, posterior cerebral artery).

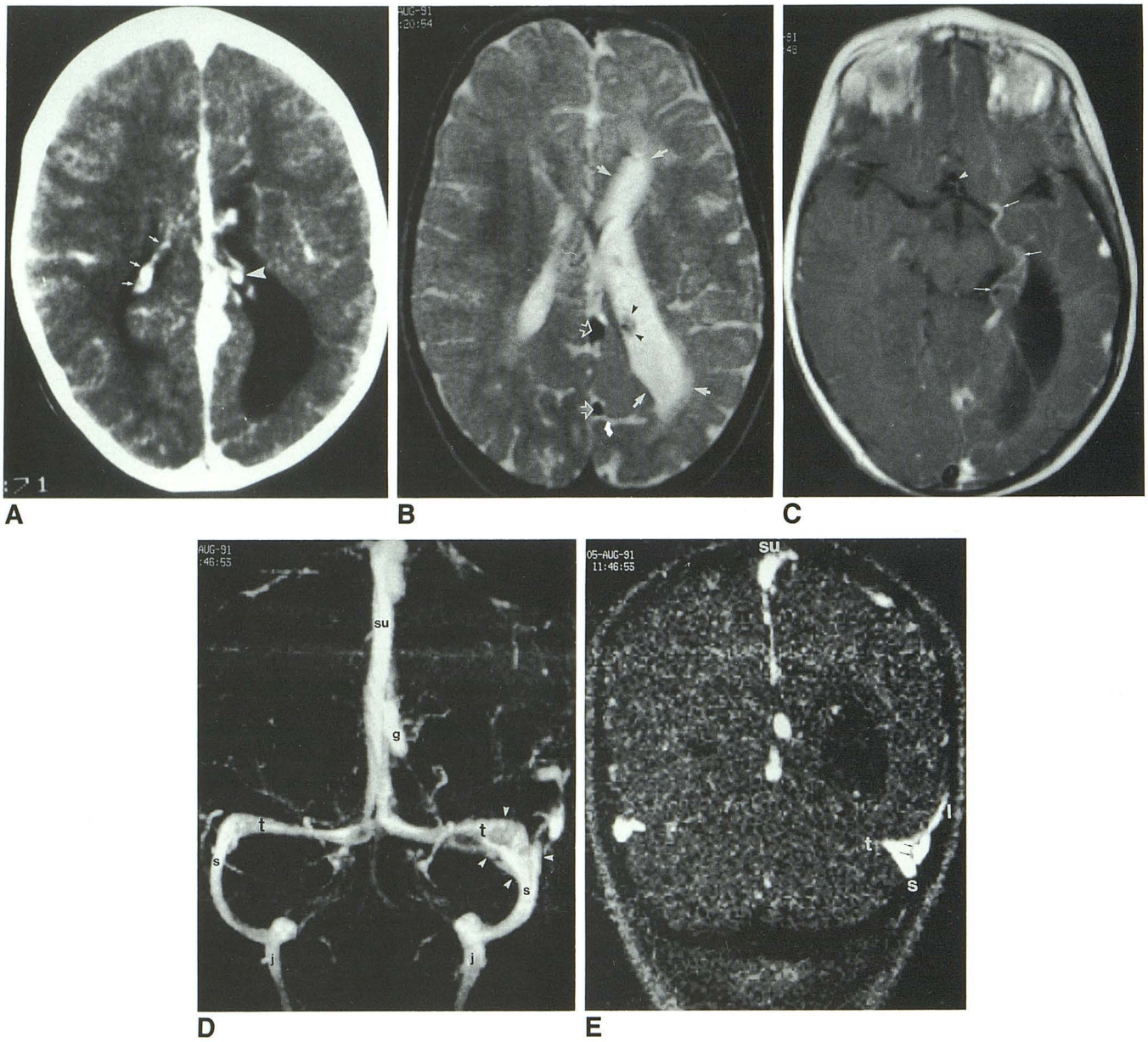

Fig. 4. Case 4. This 2-year-old patient presented with multiple nevi and right-sided seizures.

A, CT scan, enhanced image; this enhanced CT scan demonstrates calcification of the glomus of the choroid plexus (*arrowhead*). Note the enlarged glomus of the choroid plexus (*arrows*), the volume loss and dilated ventricle system of the left hemisphere, and the spotty enhancement of cortical areas.

B, SE, T2-weighted, 2500/90 TR/TE, plain, axial image; the T2-weighted image demonstrates the choroid plexus calcification as an area of decreased signal intensity (*black arrowheads*). Note the engorged deep venous system (*open arrows*), and the dilated left ventricle (*white arrows*).

C, SE, T1-weighted, Gd-DTPA, plain, axial image; this view shows several engorged deep veins (*arrowhead*), a dilated left ventricle, and a vessel with high signal intensity on the T1-weighted scan (*arrows*), suggesting slow flow in this vessel.

D, Venous MRA, FLASH 2D, 36/10, $\alpha = 60°$, coronal image; the coronal view of the angiogram shows a lack of superficial veins, a prominent vein of Galen (*g*) and an enlargement of the left transverse sinus passing into the sigmoid sinus (*arrowheads*) (*su*, superior sagittal sinus; *g*, vein of Galen; *t*, transverse sinus; *s*, sigmoid sinus; *j*, jugular vein).

E, Venous MRA, FLASH 2D, 36/10, $\alpha = 60°$, coronal image; this individual section from venous MRA reveals an engorged left transverse and sigmoid sinus with a septum visible at the junction of the engorged vein of Labbé (*black arrows*) (*su*, superior sagittal sinus; *t*, transverse sinus; *s*, sigmoid sinus; *l*, vein of Labbé).

tomical sources of flow. In one of our patients, a septum in the sigmoid sinus could be clearly delineated in the individual sections of venous MRA (Fig. 4E); such septae can occasionally suggest a false positive diagnosis of dural sinus thrombosis in conventional angiography and reconstructed MR angiograms.

We tried to visualize directly the vascular pathology of Sturge-Weber syndrome by using arterial and venous MRA, since the advantage of these sequences is in allowing the visualization of flow in engorged vessels, seen on SE images as areas of signal void. If vascular anomalies are suspected on a routine MR examination, MRA is able to demonstrate the extension of the angiomatous changes, and can depict the involved vessels. Additionally, MRA offers the possibility of demonstrating signal loss, thus giving information about slow cerebral venous drainage, sinus thrombosis, or arterial stenosis. MRA sequences are quickly performed, each being about 7 minutes, and can thus be easily added to a routine examination. While we find venous MRA to be highly sensitive in revealing the typical medullary vascular changes of Sturge-Weber syndrome, we find that arterial MRA is helpful in showing the changes in the higher cortical branches of affected vessels, albeit much more subtly. The direct visualization of the pathologic arterial and venous flow patterns are not unimportant, since some groups are engaged in surgical treatment in cases of therapy refractory seizures in Sturge-Weber syndrome (15–17).

We find that MRA in combination with MR imaging can give detailed information regarding vascular anomalies, while being less invasive than conventional techniques. MRA can be helpful in gauging the extent of cerebral involvement in children with facial nevus, for example, in cases where seizures have not yet been documented and there is doubt as to whether the diagnosis of Sturge-Weber is correct. In conclusion, arterial and venous MR can be useful adjuncts to standard SE sequences in diagnosing Sturge-Weber syndrome.

Acknowledgment

We would to thank Professor Derek Harwood-Nash for his valuable assistance in preparing this article.

References

1. Boltshauser E, Wilson J, Hoare RD. Sturge-Weber syndrome with bilateral intracranial calcifications. *J Neurol Neurosurg Psychiatry* 1976;39:429–435
2. Aicardi J, Chevrie JJ. Consequences of status epilepticus in infants and children. In: Delgado-Escueta AV, Wasterlain CG, Treiman DM, Porter RJ, eds. *Adv neurol* 1983;34:115–125
3. Adams JH, Corellis JAN, Duchen LW. *Greenfield's neuropathology*. 4th ed. New York: Wiley, 1986:431
4. New PFJ, Scott WR. *Computed tomography of the brain and orbit*. Baltimore: Williams & Wilkins, 1975:421–423
5. Atlas SW, Grossman RI, Hackney DB, et al. Calcified intracranial lesions: detection with gradient-echo-acquisition rapid MR imaging. *AJNR* 1988;9:253–259
6. Wasenko JJ, Rosenbloom SA, Duchesneau PM, Lanzierl CF, Weinstein MA. The Sturge-Weber syndrome: comparison of MR and CT characteristics. *AJNR* 1990;11:131–134
7. Stimac GK, Soloman MA, Newton TH. CT and MR of angiomatous malformations of the choroid plexus in patients with Sturge-Weber disease. *AJNR* 1986;7:623–627
8. Wagner EJ, Rao KC, Knipp HC. CT-angiographic correlation in Sturge-Weber syndrome. *J Comput Assist Tomogr* 1981;5:324–327
9. Lipski S, Brunelle F, Aicardi J, Hirsch JF, Lallemand D. Gd-DOTA-enhanced MR imaging in two cases of Sturge-Weber syndrome. *AJNR* 1990;11:690–692
10. Alexander GL. Sturge-Weber syndrome. In: Vinken PJ, Bruyn YN, eds. *Handbook of clinical neurology*. Vol 14. *The phakomatoses*. Amsterdam: North Holland, 1972:223–240
11. Verity CM, Strauss EH, Moyes PD, Wada JA, Dunn HG, Lavointe JS. Long-term follow-up after cerebral hemispherectomy: neurophysiologic, radiologic and psychological findings. *Neurology* 1982;32:629–639
12. Gomez MR, Begin M. Seizures and mental development in patients with Sturge-Weber disease (abstr). *J Child Neurol* 1986;1:263
13. Poser GM, Taveras JM. Cerebral angiography in encephalotrigeminal angiomatosis. *Radiology* 1957;68:327–336
14. Probst FP. Vascular morphology and angiographic flow patterns in Sturge-Weber angiomatosis: facts, thoughts and suggestions. *Neuroradiology* 1980;7:73–78
15. Bentson JR, Wilson GH, Newton TH. Cerebral venous drainage pattern of the Sturbe-Weber syndrome. *Radiology* 1971;101:111–118
16. Rosen I, Salford L, Starck L. Sturge-Weber disease: neurophysiological evaluation of a case with secondary epileptogenesis, successfully treated with lobe-ectomy. *Neuropediatrics* 1984;15:95–98
17. Ito M, Sato K, Maruki C, Nitta T, Ohnuki A, Ishii S. Surgical treatment of Sturge-Weber syndrome-case report. *Neurol Med Chir (Tokyo)* 1989;29:60–64